# Simultaneous Identification and Torque Control of Surface-Mount Permanent Magnet Synchronous Machines with Inverter Current and Voltage Constraints

Fanny A. Pinto Delgado, David M. Reed, Heath F. Hofmann, and Jing Sun

***Abstract*— In variable-speed drive applications, the system will have constraints on the line currents and voltages due to limitations of both the machine and the power electronic circuitry driving the machine. This paper presents a Simultaneous Identification and Control (SIC) methodology for Surface-Mount Permanent Magnet (SMPM) machines including voltage and current constraints. The over-actuated nature of the SMPM is exploited to achieve both control and parameter identification objectives without compromise. An optimization-based adaptive input design methodology aims to minimize control effort and maximize the excitation characteristics of the generated reference direct-axis current trajectories within the voltage and current constraints. The optimized current command is fed into an adaptive current regulator to achieve torque control. Simulation results demonstrate that the constraint enforcement capability of the proposed SIC algorithm allows the machine to achieve the desired control and identification objectives while operating in current-constrained, voltage-constrained, and current-and-voltage-constrained conditions.**

## I. Introduction

Simultaneous Identification and Control (SIC) refers to control methodologies that aim to achieve control objectives while also guaranteeing sufficient conditions for accurate parameter identification. Accurate parameter identification is often desirable since it can be used for control adaptation to achieve improved performance and other secondary objectives, such as condition monitoring [1]. However, accurate parameter identification requires persistently exciting inputs (i.e., signals rich in harmonics) [2] which may conflict with the control goal (e.g., a set-point or trajectory that the controller tries to track). Because of the competing objectives between identification and control, the SIC problem is often approached through optimization-based design methodologies such as Model Predictive Control (MPC) [3]–[7]. Although a trade-off is unavoidable for most plants, for over-actuated plants, where the number of control inputs exceeds the number of regulated outputs, this additional degree of freedom can be exploited to simultaneously achieve identification and control objectives without compromise [8]–[13].

An example of an over-actuated system is the Permanent Magnet Synchronous Machine (PMSM), which effectively has two inputs (i.e., equivalent two-phase voltages) and a single regulated output (i.e., torque). Surface-Mount Permanent Magnet (SMPM) machines and Interior Permanent Magnet (IPM) machines are the two main types of PMSMs and have been widely used in a variety of applications, such as electric vehicles and wind turbines, due to their high torque density and efficiency. However, the performance of model-based PMSM controllers can deteriorate depending on operating conditions since variations in temperature, skin effect, and magnetic saturation can cause the machine parameters to vary. In the literature, many online methods have been proposed to incorporate machine parameter identification for adaptation [11]–[17]. Specifically, the methodologies presented in [11]–[13] exploit the over-actuated characteristic of the PMSMs for SIC.

Operational constraints are inherent in PMSMs due to physical limitations as well as safety and reliability considerations. In an electric drive, which is used to provide power to the PMSM, a three-phase Voltage Source Inverter (VSI) supplies the AC voltages in a limited range that depends on the DC bus voltage and the Pulse Width Modulation (PWM) technique used for DC-AC conversion. Commanding voltages outside this range will lead to clipped output voltages and deteriorated control performance. Furthermore, exceeding the current limit in a phase will trip the overcurrent protection of the inverter.

Space Vector Modulation (SVM) is one of the most-used PWM techniques because of its superior performance. The feasible voltage region for SVM is bounded by the well-known space vector hexagon [18]. The maximum line current constraint can also be described by a hexagon, as will be shown in the sequel. One or both of these constraints can be active depending on the operating conditions (i.e., speed and power/torque). In the case of the SMPM machine, the maximum power as a function of speed depends on the SMPM design and the inverter limits, and can have two behaviors: 1) current-constrained at low speeds, voltage-and-current-constrained at medium speeds, and voltage-constrained at high speeds, or 2) current-constrained at low speeds, and voltage-and-current-constrained up to a maximum speed [19]. To the best of the authors' knowledge, there is no previous work on SIC of PMSMs that accurately characterizes these limits and addresses them through control formulation and implementation.

In this paper, we propose an optimization-based SIC formulation that explicitly considers the voltage and current

Fanny A. Pinto Delgado and Heath F. Hofmann are with the department of Electrical Engineering and Computer Science and Jing Sun is with the department of Naval Architecture and Marine Engineering at the University of Michigan, Ann Arbor, MI 48109 USA (e-mail: fapd@umich.edu; hofmann@umich.edu; jingsun@umich.edu).

David M. Reed is with Mercedes-Benz Research and Development North America,, Redford, MI 48239 USA (e-mail: david.reed@daimler.com).

Preprint submitted to 2018 IEEE Conference on Control Technology and Applications. Received February 1, 2018.

inverter limits for the specific case of SMPM machines. By taking advantage of the over-actuated nature of the SMPM, the SIC problem is simplified in the sense that torque regulation is achieved using the quadrature component of the current, while the persistently exciting input required for accurate parameter identification is injected using the direct component. An optimization-based adaptive input design methodology is used to minimize losses and maximize the excitation characteristics while considering the voltage and current constraints. The reference direct current generated by the adaptive input design, together with the quadrature current, is then fed into a projection-based adaptive current regulator for torque control. This paper represents a significant extension of [11], since we have:

- Formulated voltage and current constraints assuming that the system is driven by an ideal VSI.
- Modified the parameter estimator from a continuous-time technique (i.e., Lyapunov-based estimator) to a discrete-time method (i.e., projection-based estimator).
- Modified the prediction model to capture the discrete-time implementation.
- Provided simulations that demonstrate the constraint enforcement capability of the methodology.

The rest of paper is organized as follows. In Section II, we review the dynamic SMPM machine model. The control objectives and current/voltage limitations are discussed in Sections III and IV respectively. In Section V, the adaptive current regulator and the adaptive input design are described. Simulation results showing the constraint enforcement capabilities when the system is operating in current-constrained, voltage-constrained, and current-and-voltage-constrained conditions are presented in Section VI. Finally, in Section VII, concluding remarks are discussed.

## II. SMPM Machine Model

The model used in this paper for SMPM machines is the standard equivalent two-phase model. By applying the Park transform [20] and setting the direct-axis to be aligned with the rotor permanent magnet flux linkage, the electrical dynamics in the rotor reference frame are given by

$$\boldsymbol{L}\frac{d\vec{i}^{\,r}}{dt} = -\boldsymbol{R}\vec{i}^{\,r} - \omega_{re}\boldsymbol{J}(\boldsymbol{L}\vec{i}^{\,r} + \vec{\lambda}^{\,r}_{PM}) + \vec{v}^{\,r}, \qquad (1)$$

where the superscript $(\cdot)^r$ denotes that the variable is in the rotor reference frame, $\vec{i}$ and $\vec{v}$ are the current and voltage vectors, $\boldsymbol{R}$ is the stator winding resistance matrix (i.e., $\boldsymbol{R} = R\boldsymbol{I}$, where $\boldsymbol{I}$ is the identity matrix and $R$ the stator winding resistance), $\boldsymbol{L}$ is the stator winding self-inductance matrix (i.e., $\boldsymbol{L} = L\boldsymbol{I}$, where $L$ is the stator winding self-inductance), $\vec{\lambda}^{\,r}_{PM} = \begin{bmatrix}\Lambda_{PM} & 0\end{bmatrix}^T$ is the permanent magnet flux-linkage vector, $\omega_{re}$ is the electrical rotor speed (i.e., $\omega_{re} = \frac{P}{2}\omega_r$, where $\omega_r$ is the mechanical rotor speed and $P$ is the number of poles), and $\boldsymbol{J}$ is the counterclockwise (CCW) $90°$-rotation matrix.

In the rotor reference frame, the three-phase electromagnetic torque takes the form

$$\tau_{3ph} = \frac{3P}{4}\Lambda_{PM} i^r_q. \qquad (2)$$

## III. Control Objectives

The SMPM machine is an over-actuated system since it has equivalent two-phase voltages as inputs and torque as the regulated output. Consequently, Simultaneous Identification and Control (SIC), which aims to achieve control objectives while guaranteeing persistency of excitation, can be accomplished without compromise. However, doing so considering current and voltage constraints is a challenge.

The current and/or voltage limitations that might be encountered by the SMPM machine will depend on the operating condition (i.e., torque/power and speed). Assuming that the system is operated close to its limits (e.g., maximum power condition), three regions can be identified. At low speeds, the system will be current-constrained. In this region, since the electromotive force (EMF), which is proportional to speed, is small, the voltage limit cannot be reached. At medium speeds, the system is both current-and-voltage-constrained, and the direct current is used for field-weakening so that the voltage stays within its limits. Specifically, a negative value of $i^r_d$ is commanded to reduce the flux-linkage magnitude, and, consequently, the EMF, while $i^r_q$ is adjusted accordingly to keep the current also within its limits. At high speeds, the behavior depends on whether the currents can completely cancel the permanent magnet flux linkage. In the case that the permanent magnet flux linkage is not completely cancelled, the system will continue to be current-and-voltage-constrained until the operating point of zero power is reached, where the current is exclusively used for field-weakening purposes. In the case when the permanent magnet flux linkage is completely cancelled, the system becomes solely voltage-constrained.

The control objective is to simultaneously achieve accurate torque regulation and parameter identification over a wide range of operating conditions without exceeding the voltage and current limits. This is accomplished through a controller which consists of an optimization-based adaptive input design and an adaptive current regulator. Taking advantage of the specific over-actuated characteristic of the SMPM machine, torque regulation is achieved through the quadrature-axis current while the persistently exciting signal is injected into the direct-axis current.

## IV. Current and Voltage Constraint Formulation

In this section, the mathematical formulation of the voltage and current limitations which are inherent in an electric drive with an ideal three-phase voltage source inverter (VSI) is presented. An ideal three-phase VSI, as shown in Fig. 1, applies to the machine the voltages determined by the control algorithm in an average-value sense using Pulse-Width Modulation (PWM). We treat the transistors here as ideal switches. We also assume that the VSI is controlled using Space Vector Modulation (SVM) [18].

Preprint submitted to 2018 IEEE Conference on Control Technology and Applications. Received February 1, 2018.

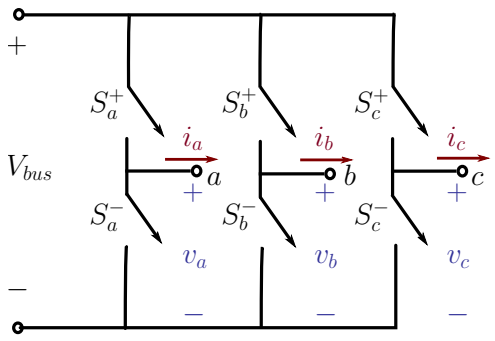


Fig. 1. Ideal three-phase inverter.

### A. Voltage Constraints

In each VSI's phase, the output voltage is a square wave with duty cycle $D$ (a.k.a., PWM signal). The calculated voltages from the controller are commanded in an average-value sense by setting the duty cycles so that the calculated voltage equals the average-value component of the VSI voltage.

The voltage constraints are formulated considering all three phases simultaneously. Each phase output voltage can have two possible states:

- State $S_x = 0$: $S_x^+$ "off", $S_x^-$ "on" $\implies$ $v_x = 0$
- State $S_x = 1$: $S_x^+$ "on", $S_x^-$ "off" $\implies$ $v_x = V_{bus}$

where the subscript $(\cdot)_x$ represents each phase (i.e., $a$, $b$, $c$). Then, using the Clarke transform [21], the equivalent two-phase voltages can be determined for all possible states $(S_a, S_b, S_c)$. The region of feasible average-value voltages is described by the interior of the hexagon presented in Fig. 2, which is the well-known "space vector hexagon" [18].

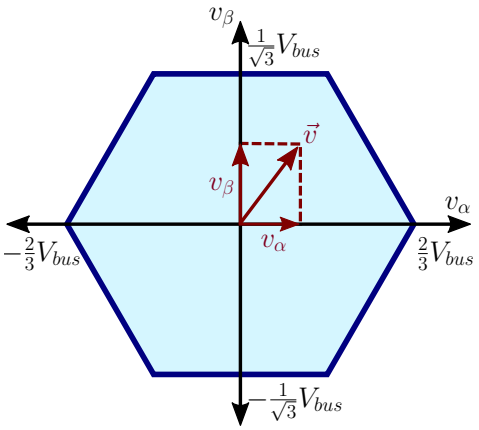


Fig. 2. Region of feasible voltages.

The interior of this hexagon can be represented mathematically by the following set, $\Omega_v$:

$$\Omega_v = \{\vec{v} : \boldsymbol{G_v}\vec{v} \leq \vec{h}_v\}, \tag{3}$$

where

$$\boldsymbol{G_v} = \begin{bmatrix} 0 & 1 \\ 0 & -1 \\ -\sqrt{3} & 1 \\ \sqrt{3} & 1 \\ -\sqrt{3} & -1 \\ \sqrt{3} & -1 \end{bmatrix}, \vec{h}_v = -\begin{bmatrix} 1 \\ 1 \\ 2 \\ 2 \\ 2 \\ 2 \end{bmatrix} \frac{V_{bus}}{\sqrt{3}},$$

and $\vec{v} = \begin{bmatrix} v_\alpha & v_\beta \end{bmatrix}^T$ is the equivalent two-phase stator voltage vector in the stationary reference frame.

### B. Current Constraints

The VSI is operating at its current limit when the maximum rated current is flowing in any of its three phases. Given $i_\alpha$ and $i_\beta$ (i.e., the components of the equivalent two-phase current), the three-phase line currents can be expressed as [21]:

$$\begin{aligned} i_a &= i_\alpha + i_0, \\ i_b &= -\frac{1}{2}i_\alpha + \frac{\sqrt{3}}{2}i_\beta + i_0, \\ i_c &= -\frac{1}{2}i_\alpha - \frac{\sqrt{3}}{2}i_\beta + i_0, \end{aligned} \tag{4}$$

where $i_0$ is the zero sequence current component. Thus, the line current constraints can be expressed as:

$$\begin{aligned} -I_{max} \leq i_\alpha + i_0 \leq I_{max}, \\ -I_{max} \leq -\frac{1}{2}i_\alpha + \frac{\sqrt{3}}{2}i_\beta + i_0 \leq I_{max}, \\ -I_{max} \leq -\frac{1}{2}i_\alpha - \frac{\sqrt{3}}{2}i_\beta + i_0 \leq I_{max}, \end{aligned} \tag{5}$$

where $I_{max}$ is the maximum line current amplitude. Assuming balanced three-phase operation (i.e., $i_0 = 0$), the limits of the feasible current region in terms of the equivalent two-phase currents (i.e., $i_\alpha$, $i_\beta$) corresponds to the hexagon presented in Fig. 3.

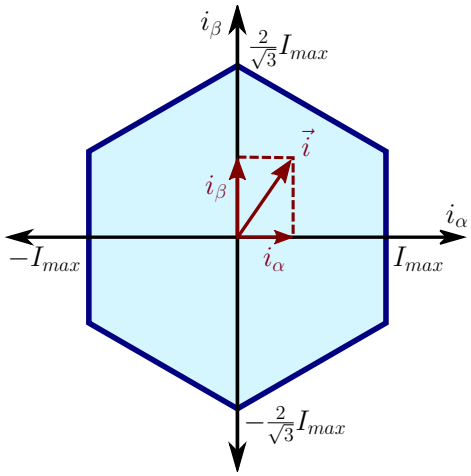


Fig. 3. Region of feasible currents.

This region can, therefore, be characterized by the following set, $\Omega_i$:

$$\Omega_i = \{\vec{i} : \boldsymbol{G_i}\vec{i} \leq \vec{h}_i\}, \tag{6}$$

Preprint submitted to 2018 IEEE Conference on Control Technology and Applications. Received February 1, 2018.

where

$$\boldsymbol{G_i} = \begin{bmatrix} 1 & 0 \\ -1 & 0 \\ -\frac{1}{\sqrt{3}} & 1 \\ \frac{1}{\sqrt{3}} & 1 \\ -\frac{1}{\sqrt{3}} & -1 \\ \frac{1}{\sqrt{3}} & -1 \end{bmatrix}, \vec{h}_i = - \begin{bmatrix} 1 \\ 1 \\ \frac{2}{\sqrt{3}} \\ \frac{2}{\sqrt{3}} \\ \frac{2}{\sqrt{3}} \\ \frac{2}{\sqrt{3}} \end{bmatrix} I_{max}.$$

## V. Control Algorithm

The proposed SIC methodology, which is an extension of [11], uses an optimization-based adaptive input design and an adaptive current regulator, as shown in Fig. 4. While the reference quadrature current is set to achieve the desired torque, the optimization-based adaptive input design ensures persistency of excitation, a sufficient condition for parameter convergence, by generating an appropriate reference direct current. These reference currents are then fed into the adaptive current regulator.

### A. Adaptive Current Regulator

The controller consists of a projection-based adaptive current regulator. The control law is a combination of feedforward, back-emf compensation, and proportional feedback, and is given by

$$\vec{v}^r = \hat{\boldsymbol{R}}\tilde{\vec{i}}^r + \hat{\boldsymbol{L}}\frac{d\tilde{\vec{i}}^r}{dt} + \omega_{re}\boldsymbol{J}(\hat{\boldsymbol{L}}\vec{i}^r + \hat{\vec{\lambda}}_{PM}) + \boldsymbol{K_p}\vec{e}_i{}^r, \quad (7)$$

where the accent $(\hat{\cdot})$ denotes an estimated parameter, $\tilde{\vec{i}}^r$ is the filtered reference current vector ( i.e., $\tilde{\vec{i}}^r = \{M(s)\}\vec{i}^{*r}$, where $\vec{i}^{*r}$ is the reference current vector, $\{\cdot\}$ denotes a dynamic operator with transfer function " $\cdot$ ", and $M(s) = \frac{\lambda}{s+\lambda}$), $\frac{d\tilde{\vec{i}}^r}{dt} = \{sM(s)\}\vec{i}^{*r}$ is the derivative of the filtered reference current vector, $\boldsymbol{K_p}$ is the proportional feedback gain matrix (i.e., $\boldsymbol{K_p} = K_p\boldsymbol{I}$, where $K_p$ is the proportional feedback gain), and $\vec{e}_i{}^r = \begin{bmatrix} e^r_{i_d} & e^r_{i_q} \end{bmatrix}^T$ is the stator current error vector, which is defined as the difference between the filtered reference current and the measured current (i.e., $\vec{e}_i{}^r = \tilde{\vec{i}}^r - \vec{i}^r$).

The adaptive law is based on the linear parameterization of the filtered SMPM dynamics (1):

$$\vec{z} = \boldsymbol{\Phi}^T\vec{\theta}, \quad (8)$$

where $\vec{z} = \begin{bmatrix} z_d & z_q \end{bmatrix}^T = \{M(s)\}\vec{v}^r$ is the observation (i.e., measurement), $\vec{\theta} = \begin{bmatrix} R & L & \Lambda_{PM} \end{bmatrix}^T$ is the parameter vector, and $\boldsymbol{\Phi}$ is the regressor matrix, which is given by

$$\boldsymbol{\Phi}^T = \begin{bmatrix} \vec{\phi}_d^{\,T} \\ \vec{\phi}_q^{\,T} \end{bmatrix} = \{M(s)\} \begin{bmatrix} i^r_d & (\frac{d}{dt}i^r_d - \omega_{re}i^r_q) & 0 \\ i^r_q & (\omega_{re}i^r_d + \frac{d}{dt}i^r_q) & \omega_{re} \end{bmatrix}. \quad (9)$$

Note that the dynamics have been filtered in order to avoid the derivatives appearing as signals in $\boldsymbol{\Phi}$ or $\vec{z}$.

While the control formulation and design are carried out with a continuous-time model, parameter identification and update are performed at discrete time instants. The projection algorithm [22] aims to minimize the Euclidean norm between consecutive parameter estimates subject to the model in (8), and its estimated parameters are given by,

$$\hat{\vec{\theta}}[k] = \hat{\vec{\theta}}[k-1] + \frac{a\vec{\phi}_d[k]\big(z_d[k] - \hat{\vec{\theta}}[k-1]\vec{\phi}_d^{\,T}[k]\big)}{c + \vec{\phi}_d^{\,T}[k]\vec{\phi}_d[k]} + \frac{a\vec{\phi}_q[k]\big(z_q[k] - \hat{\vec{\theta}}[k-1]\vec{\phi}_q^{\,T}[k]\big)}{c + \vec{\phi}_q^{\,T}[k]\vec{\phi}_q[k]}, \quad (10)$$

where $c > 0$ is a small constant used to avoid division by zero, $0 < a < 2$ is the adaption gain, and $k = 1, 2, ...$ is the time index.

### B. Receding Horizon Adaptive Input Design

The Receding Horizon Adaptive Input Design (RHAID) methodology determines the reference direct current trajectory based on two objectives: minimizing ohmic losses and maximizing the level of excitation. While the metric for minimizing losses is the weighted quadratic function of the reference direct current, the level of persistency of excitation is measured using the "D-optimality" metric [23]:

$$J_D = \log(\det(\boldsymbol{F})), \quad (11)$$

where $\mathbf{F}$ is the Fisher information matrix [11], which is given by

$$\boldsymbol{F} = \sum_{k=1}^{N} \boldsymbol{\Phi}(t_k)\boldsymbol{\Phi}^T(t_k), \quad (12)$$

where $\boldsymbol{\Phi}(t_k)$ is the regressor matrix at time $t_k$, and $N$ is the total number of observations (i.e., measurements).

In order to implement the RHAID, the future states of the system have to be predicted, and a dynamical model of the system is required. Since the actual implementation is in discrete time, this model is formulated using the Zero-Order Hold (ZOH) equivalent model of the continuous-time dynamics presented in (1), and takes into account the intrinsic switching-period delay between measurement sampling and duty cycle updates. Since the true parameters are unknown, the model uses the certainty equivalence principle [2] which assumes that the estimated and actual parameters are equal. Note that the control law in (7) uses the filtered reference signals and their derivatives, and, therefore, the model has to consider the dynamics of $\{M(s)\}$ and $\{sM(s)\}$. Then, the prediction model is given by the following discrete-time state-space system,

$$\vec{x}[k+1] = \hat{\boldsymbol{A}}_{\boldsymbol{d}}\vec{x}[k] + \boldsymbol{B_d}\vec{u}[k], \quad (13)$$

where

$$\hat{\boldsymbol{A}}_{\boldsymbol{d}} = \begin{bmatrix} e^{\hat{\boldsymbol{A}}T_{sw}} & \hat{\boldsymbol{B}}(\omega_{re}\boldsymbol{J}\hat{\boldsymbol{L}} - \boldsymbol{K_p}) & \hat{\boldsymbol{B}}(\hat{\boldsymbol{R}} + \boldsymbol{K_p}) & \hat{\boldsymbol{B}}\hat{\boldsymbol{L}} \\ \boldsymbol{I} & \boldsymbol{0} & \boldsymbol{0} & \boldsymbol{0} \\ \boldsymbol{0} & \boldsymbol{0} & a_f\boldsymbol{I} & \boldsymbol{0} \\ \boldsymbol{0} & \boldsymbol{0} & \boldsymbol{0} & a_f\boldsymbol{I} \end{bmatrix},$$

$$\boldsymbol{B_d} = \begin{bmatrix} \boldsymbol{0} & \boldsymbol{0} \\ \boldsymbol{0} & \boldsymbol{0} \\ \boldsymbol{0} & b_f\boldsymbol{I} \\ \lambda\boldsymbol{I} & -\lambda\boldsymbol{I} \end{bmatrix}, \vec{x}[k] = \begin{bmatrix} \vec{i}^r[k] \\ \vec{i}^r[k-1] \\ \tilde{\vec{i}}^r[k] \\ \frac{d\tilde{\vec{i}}^r}{dt}[k] \end{bmatrix},$$

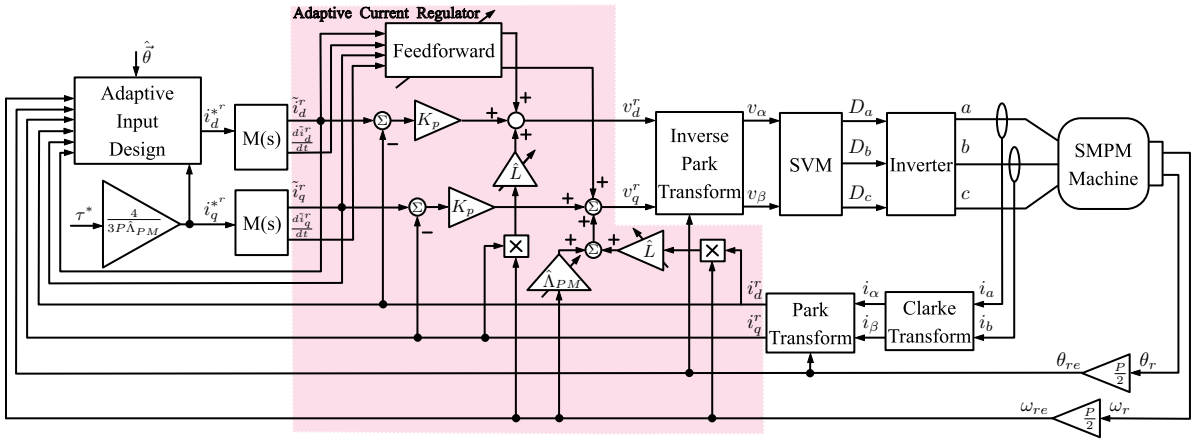


Fig. 4. Block diagram of the proposed simultaneous identification and control strategy.

$$\vec{u}[k] = \begin{bmatrix} \vec{i}^{r^*}[k+1] \\ \vec{i}^{r^*}[k] \end{bmatrix}, \hat{\boldsymbol{A}} = \boldsymbol{L^{-1}}(\boldsymbol{R} + \omega_{re}\boldsymbol{JL}),$$

$\hat{\boldsymbol{B}} = (e^{\hat{\boldsymbol{A}}_{\boldsymbol{d}} T_{sw}} - \boldsymbol{I})(\hat{\boldsymbol{R}} + w_{re}\boldsymbol{J}\hat{\boldsymbol{L}})^{-1}$, $\lambda > 0$ is the continuous-time parameter of the first-order filter ( i.e., $M(s) = \frac{\lambda}{s+\lambda}$ ), $T_{sw}$ is the sampling period, and $a_f$ and $b_f$ are the parameters of the ZOH equivalent model of the continuous-time first-order filter, $\{M(s)\}$ ( i.e., $M(z) = \frac{b_f}{z - a_f}$ with $a_f = e^{-\lambda T_{sw}}$ and $b_f = 1 - e^{-\lambda T_{sw}}$). Note that $\tilde{\vec{i}}^r[k]$ and $\frac{d\tilde{\vec{i}}^r}{dt}[k]$ are the outputs from the ZOH equivalent model of the continuous-time first order filters $\{M(s)\}$ and $\{sM(s)\}$, respectively. We need both $\vec{i}^r[k]$ and $\vec{i}^r[k-1]$ as states of $\vec{x}[k]$ to incorporate the effect of the switching-period delay between measurement sampling and duty cycle updates.

Assuming that the estimated parameters $\hat{\vec{\theta}}[k]$, the torque reference $\tau^*[k]$, and the rotor electrical speed $\omega_{re}[k]$ are essentially constant over the prediction horizon, the RHAID formulation is given by

$$\begin{aligned}
\min_{i_d^{r^*}[k]} \quad & \sum_{k=j}^{j+N_f-1} w \cdot \left(i_d^{r^*}[k]\right)^2 - \rho \cdot \log(\det(\boldsymbol{F}(\vec{x})), \\
\text{subject to:} \quad & \vec{x}[k+1] = \hat{\boldsymbol{A}}_{\boldsymbol{d}}\vec{x}[k] + \boldsymbol{B_d}\vec{u}[k], \\
& \boldsymbol{F}(\vec{x}) = \sum_{k=j-N_p}^{j+N_f-1} \boldsymbol{\Phi}(\vec{x}[k])\boldsymbol{\Phi}(\vec{x}[k])^T, \\
& \boldsymbol{G_i} e^{\mathbf{J}\theta_{re}[k]} \tilde{\vec{i}}^r[k] \leq \vec{h}_i \ \forall k \epsilon [j \ldots j+N_f-1], \\
& \boldsymbol{G_v} e^{\mathbf{J}\theta_{re}[k]} \vec{v}^r[k] \leq \vec{h}_v \ \forall k \epsilon [j \ldots j+N_f-1], \\
& \vec{i}^{r^*}[k] = \begin{bmatrix} i_d^{r^*}[k] \\ i_q^{r^*}[k] \end{bmatrix} = \begin{bmatrix} i_d^{*^r}[k] \\ \frac{4\tau^*[k]}{3P\hat{\Lambda}_{PM}} \end{bmatrix},
\end{aligned} \tag{14}$$

where $w > 0$ and $\rho \geq 0$ are the weightings for the control effort metric and PE metric, respectively, $N_f$ is the prediction horizon, $N_p$ is the number of past-data points which are required to achieve persistently exciting reference currents (as discussed in [11]), $e^{\mathbf{J}\theta_{re}[k]}$ is a matrix exponential, and $\theta_{re}[k]$ is the predicted electrical rotor position at time $t_k$, which is determined here by

$$\theta_{re}[k] = \theta_{re}[j] + \left[\frac{1}{2} + (k-j)\right]\omega_{re}[k]T_{sw}, \forall k \neq j. \tag{15}$$

Note that, in (14), the inverse Park transform [20] (i.e., $e^{\mathbf{J}\theta_{re}[k]}$) is used to convert the currents and voltages from the rotor reference frame into the stationary frame (i.e., $\alpha - \beta$ coordinates) since the voltage and current constraints are formulated in this frame.

## VI. Simulation Results

The constraint enforcement capability of the proposed SIC algorithm at operating points close to the VSI limits is validated by numerical simulations using Matlab/Simulink. The methodology is tested at three operating conditions: low speed (current-constrained), medium speed (current-and-voltage-constrained), and high speed (voltage-constrained), representing the three limiting regions discussed for SMPM drives.

TABLE I
Simulation Parameters.

| Description | Value |
|---|---|
| Electrical Machine Parameters: | |
| $R$ | $436\,m\Omega$ |
| $L$ | $2\,mH$ |
| $\Lambda_{PM}$ | $12.579\,mV \cdot s$ |
| $P$ | 10 |
| VSI Parameters: | |
| $I_{max}$ | $7\,A$ |
| $V_{bus}$ | $30\,V$ |
| Control Design Parameters: | |
| $K_p$ | 8 |
| $a$ | 0.005 |
| $c$ | 1 |
| $\rho$ | 10 |
| $w$ | 0.01 |
| $\lambda$ | 600 |
| $N_f$ | 50 |
| $N_p$ | 60 |

The simulations capture the sampled-data nature of a practical implementation by modeling the controller (i.e., RHAID and adaptive current regulator) as a triggered subsystem

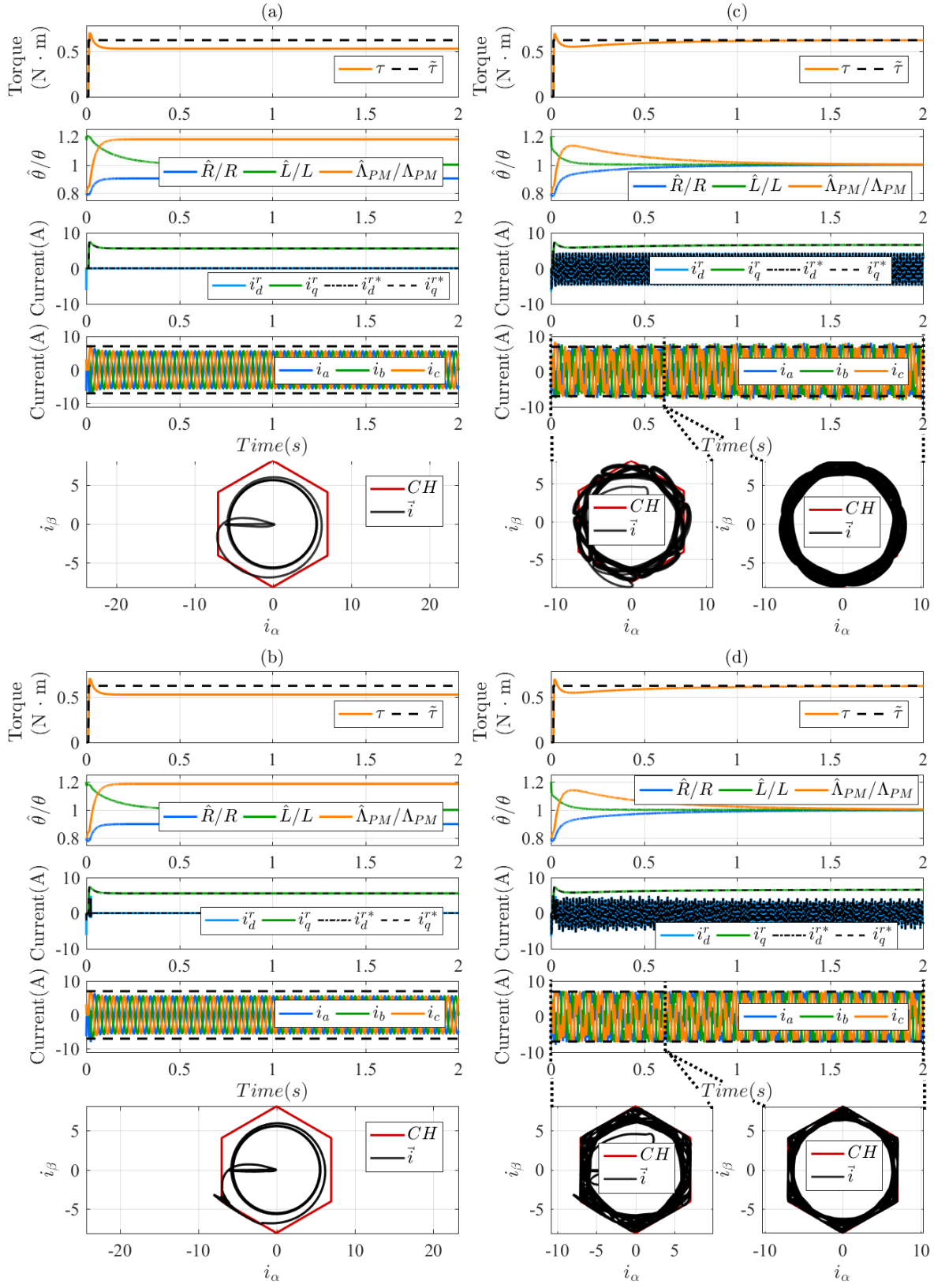


Fig. 5. Simulation results for system operating at current-constrained (low-speed) operating point assuming four different control settings. Case (a) shows the performance of the SIC methodology when no PE signal is used and current and voltage constraints are not taken into account in the RHAID. Case (b) shows the performance of the SIC methodology when no PE signal is used and current and voltage constraints are taken into account. Case (c) presents the performance when the RHAID generates the PE signal without considering current and voltage constraints. Case (d) shows the performance of the proposed SIC methodology when the RHAID produces the PE signal while considering the current and voltage constraints. Note that, for cases (c) and (d), the phase plots are presented before and after the estimated parameters reach a bound of $\pm 5\%$ from their true values

which runs at 10kHz, while the continuous-time SMPM dynamics are simulated with a fixed time step of 500ns using *ode3*. The optimization problem for the RHAID is solved using the interior-point method in Matlab's *fmincon*. A linear B-spline [4] is used to approximate the reference direct current trajectory and reduce the dimension of the optimization problem. Space Vector Modulation (SVM) is used to determine the three-phase duty cycles to be applied to the inverter based on the equivalent two-phase voltages and the DC bus voltage. An ideal "average-value" inverter is assumed, which applies to the SMPM model the average-value voltages based on the duty cycles determined by the SVM (i.e., switching harmonics are neglected). Table I presents the parameters used in the simulations.

### A. Effects of PE Signal and Constraint Enforcement

In order to highlight the impact of the PE signal and constraint enforcement on the proposed methodology, simulation results of the system operating at a current-constrained (i.e., low-speed) operating point ($200\,RPM, 0.62N{\cdot}m$) with four different control settings are presented in Fig 5. Note that, in all the cases, the initial estimated parameters differ by $20\%$ from the true values. The reference lines (black dashed) in the three-phase stator currents plots represent the line current limits. In the phase plots for the equivalent two-phase currents, "CH" denotes the current hexagon.

In Fig. 5(a), the results correspond to the case where the SIC methodology works without PE signal (i.e., $\rho = 0$) and without current/voltage constraints. As we can see from the figure, the parameters converge to the wrong values, and, consequently, the torque presents steady state error. While the projection algorithm guarantees that the error of the filtered electrical dynamics will eventually settle to zero, the parameters will only converge to their true values when the system is persistently excited (PE). Fig. 5(b) shows the results when RHAID includes the current and voltage constraints but not the PE metric (i.e., $\rho = 0$). As before, the torque presents steady-state error since the parameters converge to the wrong values. In Fig. 5(c), simulation results of the SIC methodology are presented when the RHAID generates reference direct currents that are PE (i.e., $\rho \neq 0$) but that do not take into account the current and voltage limits. As opposed to the previous case, the parameters converge to their true values and accurate torque regulation is achieved. Also note that the PE signal does not affect torque regulation. However, since the current limits were not taken into account, the constraints were violated.

### B. Constraint enforcement in three operating conditions

Figs. 5(d) , 6, and 7 show the effectiveness of the proposed algorithm in the following three conditions:

- Current constrained (Fig. 5(d)). The system provides $0.62N\cdot m$ at $200\,RPM$ which corresponds to a low-speed operating point. Inspection of the current phase plots reveals that the equivalent two-phase currents are successfully constrained within the limits after the parameters converge. The results demonstrate that enforcing the constraints in the equivalent two-phase currents effectively keeps the three-phase currents within the limits. Note that while the direct current is modified to satisfy the constraints, the parameters are still able to converge and accurate torque regulation is achieved.
- Voltage constrained (Fig. 6). The results present a high-speed operating point ($0.2\,N\cdot m$ at $2000\,RPM$). As before, the voltage constraints are effectively enforced after the parameters converge. The two-phase current time-plot shows that the RHAID responds to the voltage limitation by using the direct-axis current for field-weakening purposes (i.e., the average-value of $i_d^r$ is negative). The ripple in the actual torque is caused by the discrete-time implementation of the controller.
- Current and voltage constrained (Fig. 7). The system operates at medium-speed ($0.6\,N{\cdot}m$ at $1300\,RPM$).The voltage and current phase plots show that the equivalent two-phase voltages and currents stay within their feasible regions. Torque regulation becomes precise as the parameters approach their true values.

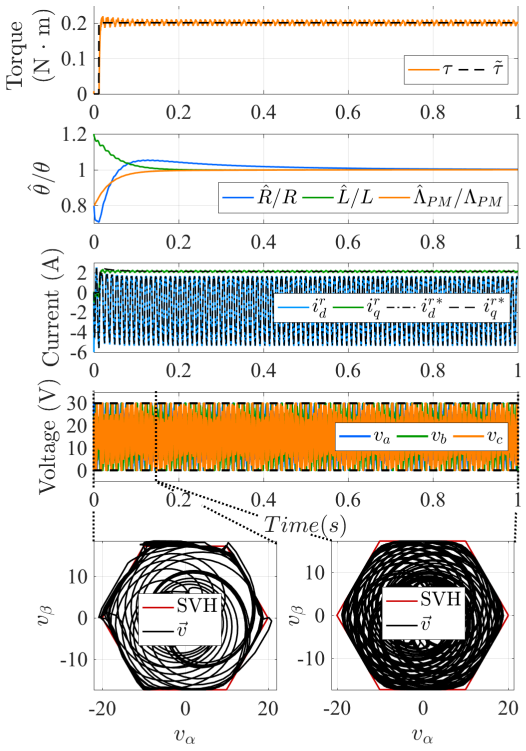


Fig. 6. Simulation results for machine operating at voltage-constrained (high-speed) operating point.

Note that the reference lines (black dashed lines) in the plot for the three-phase stator voltages represent the VSI voltage limits (i.e., zero and DC bus voltage). In the voltage phase plots, "SVH" refers to the space-vector voltage hexagon. The phase plots are presented before and after the parameters reach a bound of $\pm 5\%$ from the true parameters.

**Remark:** Simulation results show that voltage and current constraints can be enforced in the adaptive input design when parameter convergence is achieved. Before parameter conver-

Preprint submitted to 2018 IEEE Conference on Control Technology and Applications. Received February 1, 2018.

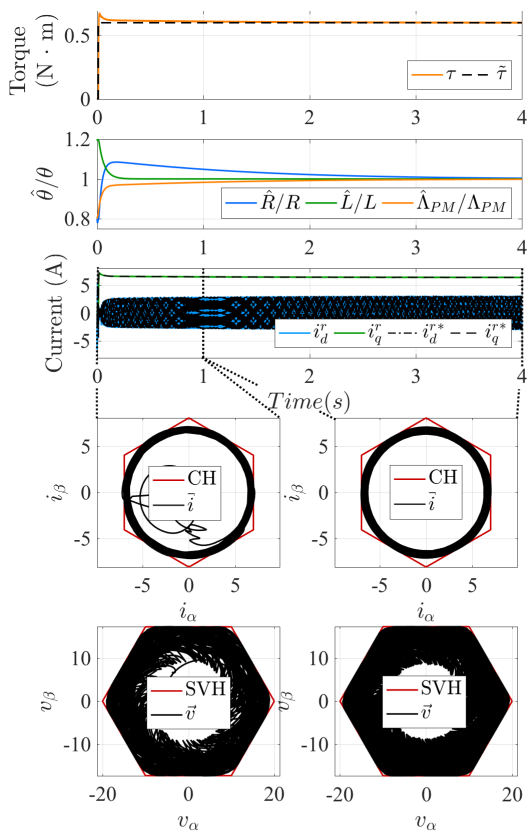


Fig. 7. Simulation results for machine operating at current-and-voltage-constrained (medium-speed) operating point.

gence, occasional constraint violations can be observed. This could be addressed by performing a calibration of parameters before use, or tightening the constraints as has been done in robust MPC [7], [24].

## VII. Conclusions

In this paper, we have presented constraints that represent the voltage and current limits of an ideal Voltage Source Inverter (VSI) and that, when included in an optimization-based SIC methodology, can be used for operation over a wide range of operating conditions (e.g., unconstrained, current-constrained, voltage-constrained, and current-and-voltage-constrained operating points) together with an effective parameter estimator. The constraints are included in an optimization-based adaptive input design that aims to minimize control effort while maximizing the excitation characteristics of the generated reference direct current trajectories. The adaptive input design feeds the computed reference currents into an adaptive current regulator. Simulation results are used to demonstrate the effectiveness of the constraints at different operating conditions.

## References

[1] K. Liu, Z. Q. Zhu, and D. A. Stone, "Parameter estimation for condition monitoring of pmsm stator winding and rotor permanent magnets," *IEEE Transactions on Industrial Electronics*, vol. 60, pp. 5902–5913, Dec 2013.

[2] P. Ioannou and J. Sun, *Robust Adaptive Control*. New Jersey: Prentice Hall, 1996.

[3] J. Rathouskỳ and V. Havlena, "Mpc-based approximate dual controller by information matrix maximization," *International Journal of Adaptive Control and Signal Processing*, vol. 27, no. 11, pp. 974–999, 2013.

[4] I. Kolmanovsky and D. P. Filev, *Optimal Finite and Receding Horizon Control for Identification in Automotive Systems*, pp. 327–348. London: Springer London, 2012.

[5] G. Marafioti, R. Bitmead, and M. Hovd, "Persistently exciting model predictive control using fir models," in *International Conference Cybernetics and Informatics*, 2010.

[6] H. Genceli and M. Nikolaou, "New approach to constrained predictive control with simultaneous model identification," *AIChE Journal*, vol. 42, no. 10, pp. 2857–2868, 1996.

[7] A. Weiss and S. D. Cairano, "Robust dual control mpc with guaranteed constraint satisfaction," in *53rd IEEE Conference on Decision and Control*, pp. 6713–6718, Dec 2014.

[8] F. Leve and M. Jah, "Spacecraft actuator alignment determination through null motion excitation," in *Proceedings of 62nd International Astronautical Congress*, 2011.

[9] A. Weiss, F. Leve, I. Kolmanovsky, and M. Jah, "Reaction wheel parameter identification and control through receding horizon-based null motion excitation," in *Bar-Itzhack Memorial Symposium*, October 2012.

[10] Y. Chen and J. Wang, "Adaptive vehicle speed control with input injections for longitudinal motion independent road frictional condition estimation," *Vehicular Technology, IEEE Transactions on*, vol. 60, pp. 839–848, March 2011.

[11] D. M. Reed, J. Sun, and H. F. Hofmann, "A receding horizon approach to simultaneous identification and torque control of permanent magnet synchronous machines," in *American Control Conference (ACC), 2016*, pp. 2211–2216, July 2016.

[12] D. M. Reed, J. Sun, and H. F. Hofmann, "A robust adaptive controller for surface-mount permanent magnet synchronous machines," in *2014 American Control Conference*, pp. 5236–5241, June 2014.

[13] D. M. Reed, J. Sun, and H. F. Hofmann, "Simultaneous identification and adaptive torque control of permanent magnet synchronous machines," *IEEE Transactions on Control Systems Technology*, vol. 25, pp. 1372–1383, July 2017.

[14] H. Kim and R. D. Lorenz, "Improved current regulators for ipm machine drives using on-line parameter estimation," in *Conference Record of the 2002 IEEE Industry Applications Conference. 37th IAS Annual Meeting (Cat. No.02CH37344)*, vol. 1, pp. 86–91 vol.1, Oct 2002.

[15] M. N. Uddin and M. M. I. Chy, "Online parameter-estimation-based speed control of pm ac motor drive in flux-weakening region," *IEEE Transactions on Industry Applications*, vol. 44, pp. 1486–1494, Sept 2008.

[16] S. Underwood and I. Husain, "Online parameter estimation and adaptive control of permanent-magnet synchronous machines," *IEEE Transactions on Industrial Electronics*, vol. 57, pp. 2435 – 2443, July 2010.

[17] H. Kim and R. Lorenz, "Improved current regulators for ipm machine drives using on-line parameter estimation," in *Industry Applications Conference, 2002. 37th IAS Annual Meeting. Conference Record of the*, vol. 1, pp. 86–91, Oct 2002.

[18] B. Bose, *Modern Power Electronics and AC Drives*. New Jersey: Prentice Hall PTR, New Jersey, 2002.

[19] K. H. Nam, *AC motor control and electrical vehicle applications*. CRC press, 2010.

[20] R. Park, "Two-reaction theory of synchronous machines, generalized method of analysis - part 1," *A.I.E.E. Transactions*, vol. 48, pp. 81–95, 1929.

[21] W. C. Duesterhoeft, M. W. Schulz, and E. Clarke, "Determination of instantaneous currents and voltages by means of alpha, beta, and zero components," *Transactions of the American Institute of Electrical Engineers*, vol. 70, pp. 1248–1255, 1951.

[22] G. Goodwin and K. Sin, *Adaptive Filtering Prediction and Control*. Dover Books on Electrical Engineering, Dover Publications, 2014.

[23] S. Silvey, *Optimal Design*. New York: Springer Netherlands, 1st ed., 1980.

[24] J. B. Rawlings and D. Q. Mayne, *Model Predictive Control: Theory and Design*. Wisconsin: Nob Hill Publishing, 2009.

Preprint submitted to 2018 IEEE Conference on Control Technology and Applications. Received February 1, 2018.